

# Quantum Neural Networks - Computational Field Theory and Dynamics

Carlos Pedro Gonçalves

March 22, 2022

Lusophone University of Humanities and Technologies, p6186@ulusofona.pt

## Abstract

To address Quantum Artificial Neural Networks as quantum dynamical computing systems, a formalization of quantum artificial neural networks as dynamical systems is developed, expanding the concept of unitary map to the neural computation setting and introducing a quantum computing field theory on the network. The formalism is illustrated in a simulation of a quantum recurrent neural network and the resulting field dynamics is researched upon, showing emergent neural waves with excitation and relaxation cycles at the level of the quantum neural activity field, as well as edge of chaos signatures, with the local neurons operating as far-from-equilibrium open quantum systems, exhibiting entropy fluctuations with complex dynamics including complex quasiperiodic patterns and power law signatures. The implications for quantum computer science, quantum complexity research, quantum technologies and neuroscience are also addressed.

**Keywords:** Quantum Artificial Neural Networks; quantum neural maps; quantum computing field theory; complex quantum systems.

# 1 Introduction

The connectionist paradigm for Artificial Intelligence (A.I.) played a key role in the development of cybernetics and the complexity sciences (Gorodkin *et al.*, 1993; Dupuy, 2000; Novikov, 2016; Ivancevic *et al.*, 2018). The dynamics of networked computational systems led, within the cybernetics paradigmatic basis, to the development of an interdisciplinary link between dynamical systems science, computer science, and evolutionary biology (Packard, 1988; Langton, 1990; Kauffman, 1990, 1991, 1993; Dupuy, 2000; Novikov, 2016; Ivancevic *et al.*, 2018).

The next generation of cybernetics is quantum cybernetics which extends the connectionist paradigm to the quantum framework, with quantum artificial neural networks (QuANNs) as a main computational model (Gonçalves, 2015a,b, 2017, 2019a,b, 2020; Novikov, 2016; Kwak *et al.*, 2021) which has recently been incorporated within the wider context of quantum machine learning (Gonçalves, 2017; Beer *et al.*, 2020; Houssein *et al.*, 2022; Parisi *et al.*, 2022).

From a quantum computer science standpoint, a QuANN with  $n$  neurons and a two-level firing pattern can be addressed as an  $n$ -qubits quantum computing network, where the quantum computing gates are conditional unitary operators that obey the network's connections, that is, the unitary quantum computing operation associated with a given neuron is conditional upon the input neurons' firing patterns, this leads to an extension of the circuit model of quantum computation applied to the quantum connectionist paradigm. Given the conditional gate structure associated with each neuron, the final quantum circuit depends upon the neuron activation sequence.

As shown in Gonçalves (2017), while a QuANN is capable of running quantum algorithms and also of selecting algorithms depending on the task, it can also operate as a quantum networked dynamical system, with the computation performed having a dynamical signature at the level of the quantum averages.

Major models of networked computation, such as cellular automata, artificial neural networks (ANNs) and random Boolean networks (Packard, 1988; Langton, 1990; Kauffman, 1990, 1991, 1993; Wolfram, 2002), when analyzed as dynamical systems led to the discovery of four major classes of behavior:

- Class 1: steady state or fixed point dynamics;
- Class 2: periodic dynamics;
- Class 3: random-like dynamics;
- Class 4: an intermediate dynamics between classes 2 and 3.

Class 4, also known as the *edge of chaos*, was a key focus of complexity research since it was shown that at the *edge of chaos* an evolutionary computing system maximized its fitness (Packard, 1988; Langton, 1990; Kauffman, 1990, 1991, 1993), also, the *edge of chaos* dynamics seem to play a role in the conditions for the emergence of complex noise resilient dynamics, since, at the *edge of chaos*, a system is able to conserve an emergent order and at the same time is capable of sustaining the necessary adaptive change (Kauffman, 1993).

In Gonçalves (2017), it was shown that QuANNs interacting with an environment can lead to complex dynamics at the level of the mean neural firing energy with *edge of chaos*-like signatures.

To research on QuANNs as quantum dynamical systems, however, we need to expand the theory to include a quantum field theory on the network, this is the main objective of the present work, which is focused on two major contributions:

1. The introduction of a complete formalism for QuANNs as quantum dynamical systems (section 2) with:
  - The definition of the networked computing formalism (subsection 2.1);

- The formalization of the concept of a unitary quantum neural map, which expands the concept of unitary quantum map, originally worked within the context of quantum chaos theory (Stöckmann, 2000; Braun, 2001; Gonçalves, 2020) (subsection 2.1);
- The expansion of quantum field theory to QuANNs, defining the concept of a quantum neural field operator, and addressing the field’s dynamics as a function of the network’s dynamics, with the formalization of recurrence analysis methods to study the quantum field dynamics on the neural network, we also exemplify the main theory with a specific field, which is the neural activity field (subsection 2.2);
- The application of von Neumann entropy to address the dynamics of each neuron as an open quantum system in connection with the network (subsection 2.3).

2. An implementation of section 2’s theoretical framework to a two-neuron quantum recurrent neural network (QRNN) and the study of the mean neural activity field’s dynamics and entropy dynamics (section 3).

As we show in section 3, for the most elementary QRNN comprised of two neurons, the quantum neural activity field’s dynamics, for different parameter values, can exhibit standard class 1 and class 2 dynamics, for other parameter values brainwave-like patterns emerge for the mean neural activity field dynamics with strongly correlated local mean field values calculated as the quantum averages for the field at each neuron, for other parameter values, the emergent dynamics is class 4.

While the whole network undergoes a unitary evolution, there are entropy fluctuations at the local neuron level, therefore, in conjunction with the analysis of the dynamics for the mean neural activity field, we study the resulting entropy sequences for each neuron, thus, treating each neuron as an open quantum system.

For different parameter values, we find that the wave-like periodic emergent pattern translates to an also emergent periodic pattern driving the local (neuron-level) entropy dynamics, while for class 4 mean neural activity field dynamics we also find class 4 dynamics in the entropy dynamics, including power law signatures at the local neuron-level entropy sequences with fluctuations never leading to maximum entropy associated with a depolarized mixed density and fluctuations that range from near zero entropy values to high but not maximum entropy, therefore, each neuron operates as a far-from-equilibrium open quantum system with no stabilized fixed decoherence pattern, a result that may be key for the development of advanced networked quantum technologies, since the local computing units do not tend to a maximum entropy and recurrently return to near zero entropy values.

The implications of the work for quantum computer science, complexity research, quantum technologies and neuroscience are addressed in section 4.

## 2 Quantum Neural Networks, Computational Field Theory and Dynamics

### 2.1 Computational Structure of Quantum Artificial Neural Networks and Quantum Neural Maps

In order to produce a general computational framework on which to discuss QuANNs, we need to consider a directed graph (digraph) structure for the  $n$  neuron network extended with a Hilbert space structure and a set of conditional unitary operators, one operator for each neuron, with the unitary computation conditional on the input neural connections, formally this digraph can be defined as follows:

**Definition 1.** (QuANN) A QuANN is a digraph with the structure:

$$G = (Q, D, \mathbb{H}_{Net}, \Theta(\mathbb{H}_{Net})), \quad (1)$$

where  $Q = \{n_0, n_1, \dots, n_{n-1}\}$  is the set of neurons,  $D$  is the set of ordered pairs corresponding to the directed edges,  $\mathbb{H}_{Net}$  is the network's Hilbert space and  $\Theta(\mathbb{H}_{Net}) = \{U_0, U_1, \dots, U_{n-1}\}$  is a set of conditional unitary operators on  $\mathbb{H}_{Net}$ , one for each neuron.

The computational dynamics of QuANNs can be addressed as a system of spinors on a network (Gonçalves, 2017). In the spinor model, when each neuron can have just two base computational patterns of activity, firing or nonfiring, corresponding to two energy levels, the Hilbert space for the full network is given by  $n$  tensor product copies of the Hilbert space  $\mathbb{H}_2$ , which is spanned by the standard qubit basis  $B_2 = \{|0\rangle, |1\rangle\}$ , where the ket vector  $|0\rangle$  represents a nonfiring neural activity and  $|1\rangle$  a firing neural activity, we are using the standard Dirac's notation where the "ket" vector  $|w\rangle$  represents a column vector and the "bra" vector  $\langle w|$  is its conjugate transpose.

The Hilbert space for the network, in the case of a binary firing pattern is defined as  $\mathbb{H}_{Net} = \mathbb{H}_2^{\otimes n}$  and spanned by the firing pattern basis (Gonçalves, 2017):

$$B_2^{\otimes n} = \{|s_0, s_1, \dots, s_{n-1}\rangle : s_k = 0, 1; k = 0, 1, \dots, n-1\} \quad (2)$$

A generalization of this model, for a finite number of logical states encoded in quantum a neural firing activity, is obtained by expanding the single neuron basis to  $B_l = \{|0\rangle, |1\rangle, \dots, |l-1\rangle\}$ , spanning the single neuron  $l$ -dimensional Hilbert space  $\mathbb{H}_l$ , which would lead to the neural network's Hilbert space  $\mathbb{H}_{Net} = \mathbb{H}_l^{\otimes n}$ , spanned by the generalized firing pattern basis:

$$B_l^{\otimes n} = \{|s_0, s_1, \dots, s_{n-1}\rangle : s_k = 0, 1, \dots, l; k = 0, 1, \dots, n-1\}, \quad (3)$$

when  $l = 2$ , this last basis reduces to the standard two-level firing pattern basis. In this section, we work with the generalized formalism, since it contains the two-level as a special case. In section 3, the example is worked for  $l = 2$ .

Now, the classical information states encoded in a neural firing dynamics, formalized as basis vectors in  $B_l^{\otimes n}$ , are not the only possible information states, we can also have a superposition of different neural firing patterns, which can be formalized as a normalized ket vector  $|\psi\rangle$  on the network's Hilbert space, expanded in the firing pattern basis as follows:

$$|\psi\rangle = \sum_{s_0, s_1, \dots, s_{n-1}} \psi(s_0, s_1, \dots, s_{n-1}) |s_0, s_1, \dots, s_{n-1}\rangle \quad (4)$$

The squared modulus of each quantum amplitude  $\psi(s_0, s_1, \dots, s_{n-1})$  provides for a statistical weight associated with each neural firing pattern, so that, for an ensemble of identical independent neural networks, the probability of the network exhibiting a specific firing pattern  $s_0, s_1, \dots, s_{n-1}$  is given by  $|\psi(s_0, s_1, \dots, s_{n-1})|^2$ .

Different interpretations of quantum mechanics interpret this statistical measure differently, for instance, in an Everettian interpretation (Everett, 1957; 1973), each alternative firing pattern with a non-zero amplitude corresponds, in this case, to a projected dimension of systemic activity, with a projective intensity coinciding with the squared norm of the projection which, in turn, corresponds to the squared modulus of the amplitude  $|\psi(s_0, s_1, \dots, s_{n-1})|^2$ , so that, considering an ensemble of identical independent neural networks all described by the same multidimensional projective pattern (the same ket vector), the ensemble density operator description leads to a statistical measure (as a relative frequency) exactly coincident with  $|\psi(s_0, s_1, \dots, s_{n-1})|^2$ , which means that, choosing at random one network in the ensemble, the probability associated with that network's exhibiting a given projected firing pattern coincides with the squared modulus of the quantum amplitudes, this point was addressed in Gonçalves (2015b).

Other interpretations of the probability link are possible (Cramer, 2016; Gonçalves, 2019a,b), we will not, however, assume here a specific interpretation quantum mechanics, with the formalism holding for different interpre-

tations. The relevant point is the link to the probabilistic description since further on we will need to work with quantum averages for quantum fields on the network that rely on the above correspondence between the squared modulus of the amplitudes and statistical weights in an ensemble of identical independent networks.

Now, quantum computations on the network are formalized by way of the operations of the unitary gates in  $\Theta(\mathbb{H}_{Net})$  on the normalized ket vectors  $|\psi\rangle$ , considering this point, in order to introduce the concept of a unitary neural map, let  $p : \{0, 1, \dots, n - 1\} \mapsto \{0, 1, \dots, n - 1\}$  represent a permutation of the neuron indices, then, we can formalize the concept of a unitary neural map as follows:

**Definition 2.** (Unitary Neural Map) A unitary neural map  $F$  is defined such that, given a permutation  $p$  of neuron indices, the map is given by the product:

$$F = U_{p(n-1)} \dots U_{p(1)} U_{p(0)} \quad (5)$$

with  $U_{p(k)} \in \Theta(\mathbb{H}_{Net})$ ,  $k = 0, 1, \dots, n - 1$ .

In this way, a unitary neural map is a product of the unitary gates in  $\Theta(\mathbb{H}_{Net})$  in an order corresponding to a neuron activation sequence that matches the permutation  $p$ . Given a unitary neural map, we can define the sequence of iterations of the map as:

$$|\psi(t)\rangle = F |\psi(t - 1)\rangle, \quad (6)$$

which expands the unitary maps, worked in quantum chaos theory (Stöckmann, 2000; Braun, 2001), to the quantum neural computational setting.

In this case,  $t$  represents the iteration step, and the QuANN's dynamics is addressed in terms of a unitary quantum map which matches the quantum computing circuit described by equation (5). Given equation (6), and letting



$|\psi(0)\rangle$  be the input for the network, we get the output at iteration  $t$  as:

$$|\psi(t)\rangle = F^t |\psi(0)\rangle \quad (7)$$

The above iteration scheme allows us to deal with QuANNs as quantum networked dynamical systems. Now, in order to better address the network's dynamics we need to introduce a quantum neural computing field theory.

## 2.2 Quantum Neural Computing Field Theory

QuANNs, when addressed as quantum networked dynamical systems, lead to a bridge between quantum field theory and quantum computing, indeed, to address QuANNs as quantum networked dynamical systems implies the need to develop a quantum field theory on the network. Working with the formalism introduced in the previous subsection, we can develop a formalism for quantum fields on the network by introducing a general quantum neural field operator  $\alpha(k)$ , as a field operator on the network, formally:

**Definition 3.** (Quantum Neural Field Operator) A quantum neural field operator on an  $n$  neurons QuANN with  $l$  firing levels  $G = (Q, D, \mathbb{H}_l^{\otimes n}, \Theta(\mathbb{H}_l^{\otimes n}))$  is a field operator  $\alpha(k)$  on the network defined with the following structure:

$$\alpha(k) = \sum_{s=0}^{l-1} \alpha_s 1_2^{\otimes(k-1)} \otimes |\alpha_s\rangle \langle \alpha_s| \otimes 1_2^{\otimes(n-k)} \quad (8)$$

where the coefficients  $\alpha_s$  are real-valued and the projectors  $|\alpha_s\rangle \langle \alpha_s|$  project over a basis  $\{|\alpha_0\rangle, |\alpha_1\rangle, \dots, |\alpha_{l-1}\rangle\}$  spanning the single neuron Hilbert space  $\mathbb{H}_l$ .

Given the above definition, it follows that the operators commute, and, for any normalized ket vector on the network of the form:

$$|\psi\rangle = |\phi\rangle \otimes |\alpha_s\rangle \otimes |\varphi\rangle \quad (9)$$

where  $|\phi\rangle \in \mathbb{H}_2^{\otimes(k-1)}$  and  $|\varphi\rangle \in \mathbb{H}_2^{\otimes(n-k)}$ , the following eigenvalue equation holds:

$$\alpha(k) |\psi\rangle = \alpha_s |\phi\rangle \otimes |\alpha_s\rangle \otimes |\varphi\rangle \quad (10)$$

for  $s = 0, 1, \dots, l$ .

Now, under the action of the quantum neural map, the field dynamics can be addressed in the Heisenberg picture as follows:

$$\alpha(k, t) = F^\dagger \alpha(k, t-1) F \quad (11)$$

Therefore, in the Heisenberg picture, the field operators undergo the unitary evolution while the vectors stay at their initial configuration, so the unitary map's iteration rule applies to the field operator rather than to the vector.

Assuming  $\alpha(k, 0) = \alpha(k)$ , recursive application of the map leads to the following link:

$$\alpha(k, t) = (F^\dagger)^t \alpha(k) (F)^t \quad (12)$$

Now, given the initial ket vector  $|\psi(0)\rangle$ , the quantum average of the field at iteration step  $t$  and at neuron  $k$ , in the Heisenberg picture, is given by:

$$\bar{\alpha}(k, t) = \langle \psi(0) | \alpha(k, t) | \psi(0) \rangle \quad (13)$$

applying equation (12) we can transition from the Heisenberg to the Schrödinger picture since:

$$\bar{\alpha}(k, t) = \langle \psi(0) | \alpha(k, t) | \psi(0) \rangle = \langle \psi(0) | (F^\dagger)^t \alpha(k) (F)^t | \psi(0) \rangle, \quad (14)$$

which leads to the equivalent result for the quantum mean field value at neuron  $k$  obtained from the quantum averages calculated in the Schrödinger picture:

$$\bar{\alpha}(k, t) = \langle \alpha(k) \rangle_t = \langle \psi(t) | \alpha(k) | \psi(t) \rangle, \quad (15)$$

so that both pictures lead to equivalent results.

Taking the sequence of real-valued quantum averages  $\langle \alpha(k) \rangle_t$ , for an  $n$  neuron network we can embed the sequence in  $\mathbb{R}^n$ , so that we get a sequence of points  $\langle \alpha \rangle_t = (\langle \alpha(0) \rangle_t, \langle \alpha(1) \rangle_t, \dots, \langle \alpha(n-1) \rangle_t)$ , which leads to a trajectory in  $\mathbb{R}^n$ .

Taking advantage of the Euclidean space metric topology of  $\mathbb{R}^n$ , for any sample path  $\{\langle \alpha \rangle_t : t = t_0, t_0 + 1, \dots, t_0 + T - 1\}$ , we can calculate the distance matrix  $\mathbf{S}$  that stores the distances for each pair of points, with entries defined as:

$$\mathbf{S}_{t,t'} = \|\langle \alpha \rangle_t - \langle \alpha \rangle_{t'}\|, \quad (16)$$

where  $\|\cdot\|$  stands for the Euclidean metric defined on  $\mathbb{R}^n$ .

The distance matrix is symmetric of rank  $T$ , with the main diagonal entries all equal to zero and it contains the information about recurrences in a sample trajectory.

Taking advantage of the Euclidean metric topology of  $\mathbb{R}^n$ , the pattern of recurrences can be extracted from the distance matrix using a closed  $\delta$ -neighborhood structure, which leads to the binary recurrence matrix  $\mathbf{R}_\delta$  with entries:

$$\mathbf{R}_{t,t'}^\delta = \begin{cases} 0, & \|\langle \alpha \rangle_t - \langle \alpha \rangle_{t'}\| > \delta \\ 1, & \|\langle \alpha \rangle_t - \langle \alpha \rangle_{t'}\| \leq \delta \end{cases} \quad (17)$$

The matrix  $\mathbf{R}_\delta$  is, thus, binary and symmetric with an entry containing the value 1 when two points in the sample trajectory are not apart from each other more than  $\delta$ , in a closed Euclidean neighborhood, which is the definition of a recurrence event, of course, given this property the diagonal of the matrix, which corresponds to the cases where  $t = t'$ , is comprised only of 1s.

We are using a closed neighborhood because it allows us to identify fully periodic dynamics since, when the dynamics is fully periodic, if the radius is set equal to zero, all diagonal lines parallel to the main diagonal corresponding to the period in question will have a value of 1 in each matrix

entry, otherwise the value will be 0. When the dynamics is not periodic there is a cutoff radius below which we do not get any recurrences. In the nonperiodic case, diagonal lines with a value of 1 in each entry, at a given radius, correspond to a periodic or quasiperiodic skeleton that the dynamics revisits, these are 100% recurrence lines, that is, lines where the percentage of points (recurrence matrix entries) that are recurrence points is equal to 100%. These lines are particularly important in identifying periodic, quasiperiodic dynamics and, even, chaotic dynamics.

For the analysis of sequences of quantum averages extracted from the iterations of the quantum neural map we calculate the following three recurrence measures (Gonçalves, 2017, 2020):

- The recurrence probability: this is the number of diagonals below the main diagonal with recurrence points, divided by the total number of diagonals below the main diagonal in the recurrence matrix, since the recurrence matrix is symmetric only the diagonals below the main diagonal are counted, in this case, this metric provides for the probability of finding a line with recurrence, in a random selection of diagonal lines below the main diagonal.
- The recurrence strength: this is the sum of the number of points that fall within a distance no greater than the radius in each diagonal, below the main diagonal, divided by the total number of diagonals below the main diagonal with recurrence, this measure evaluates how strong on average the recurrence is, if all lines with recurrence had 100% recurrence, for the radius chosen, then this number would be equal to 1, the lower this statistic is, that is, the closer to zero it is, the more interrupted the diagonals there are, which occurs for stochastic systems and also for deterministic chaotic dynamics.
- The conditional 100% recurrence probability: this is the probability that a diagonal line with recurrence has 100% recurrence, for the radius

chosen.

These recurrence statistics can be used alongside the visual analysis of a recurrence plot that plots the recurrence matrix (black and white plot) or the distance matrix (colored recurrence plot), in the black and white plot, which we will use in the present work, a point is painted in black if it is a recurrence point and white if not, this plot is a key element in addressing recurrence properties of both low and high-dimensional dynamical systems (Gonçalves, 2017, 2020; Eckmann *et al.*, 1987; Gao and Cai, 2000), and have been employed frequently in the analysis of neural network models as well as in studies on brainwave dynamics (Thomasson *et al.*, 2002; Acharya *et al.*, 2011; Aladag *et al.*, 2010; Lopes *et al.*, 2020), in Gonçalves (2017, 2020) it was also applied to QRNN simulations.

In the present work, we will apply it to the study of the behavior of the quantum neural activity field with a two-level neural firing pattern, which can be built from the fermionic raising and lowering operators on the Hilbert space  $\mathbb{H}_2$ , these raising and lowering operators are defined as:

$$a = |0\rangle\langle 1| = \begin{pmatrix} 0 & 1 \\ 0 & 0 \end{pmatrix}, \quad a^\dagger = |1\rangle\langle 0| = \begin{pmatrix} 0 & 0 \\ 1 & 0 \end{pmatrix} \quad (18)$$

For the anticommutator  $\{A, B\} = AB + BA$ , these operators obey the following relations:

$$\{a, a^\dagger\} = 1_2 = \begin{pmatrix} 1 & 0 \\ 0 & 1 \end{pmatrix} \quad (19)$$

$$\{a, a\} = \{a^\dagger, a^\dagger\} = \begin{pmatrix} 0 & 0 \\ 0 & 0 \end{pmatrix} \quad (20)$$

$$a^\dagger a |0\rangle = 0 |0\rangle \quad (21)$$

$$a^\dagger a |0\rangle = 1 |1\rangle \quad (22)$$

From the above equations, we can introduce the special case of a quantum neural field operator which is the neural activity field operator  $N$  on the network defined as:

$$N(k) = 1_2^{\otimes(k-1)} \otimes a^\dagger a \otimes 1_2^{(n-k)}, \quad (23)$$

which has the eigenvalue spectrum obeying the following equation:

$$N(k) |\dots, s_k, \dots\rangle = s_k |\dots, s_k, \dots\rangle, \quad (24)$$

thus, considering the neural firing basis, at each neuron, the field operator yields a value of 0 when the corresponding neuron is not firing (not active) and of 1 when it is firing (active).

For the sequence  $|\psi(t)\rangle$  with the expansion:

$$|\psi(t)\rangle = \sum_{s_0, s_1, \dots, s_{n-1}} \psi_t(s_0, s_1, \dots, s_{n-1}) |s_0, s_1, \dots, s_{n-1}\rangle, \quad (25)$$

the quantum averages for the neural activity field at each neuron coincide with the squared modulus of the quantum amplitudes, which coincide, in turn, with the statistical measure for the neuron to be active (firing):

$$\begin{aligned} \langle N(k) \rangle_t &= \langle \psi(t) | N(k) | \psi(t) \rangle = \\ &= 0 \sum_{s_0, \dots, s_{k-1}, s_{k+1}, \dots, s_{n-1}} |\psi(\dots, s_k = 0, \dots)|^2 + \\ &+ 1 \sum_{s_0, \dots, s_{k-1}, s_{k+1}, \dots, s_{n-1}} |\psi(\dots, s_k = 1, \dots)|^2 \\ &= \sum_{s_0, \dots, s_{k-1}, s_{k+1}, \dots, s_{n-1}} |\psi(\dots, s_k = 1, \dots)|^2 \end{aligned} \quad (26)$$

Using the  $\mathbb{R}^n$  embedding  $\langle N \rangle_t = (\langle N(0) \rangle_t, \langle N(1) \rangle_t, \dots, \langle N(n-1) \rangle_t)$ ,  $\langle N \rangle_t$  corresponds to the configuration of the mean neural activity field at each neuron. As a final point regarding the quantum neural activity field, it is

relevant to stress the relation between the neural activity field operator and the local (neuron level) neural firing energy Hamiltonian operators, formally these Hamiltonians can be defined as:

$$H_k = \omega \hbar N(k) \quad (27)$$

where  $\omega = 2\pi f$  with  $f$  corresponding to a neural firing frequency in Hertz. Given the above equations, the energy eigenvalue spectrum for the neuron is given by:

$$H_k |\dots, s_k, \dots\rangle = \omega \hbar s_k |\dots, s_k, \dots\rangle, \quad (28)$$

so that the energy is zero when the neuron is nonfiring and  $\omega \hbar$  when the neuron is firing.

These operators commute and the total neural firing energy for the network is given by:

$$H = \sum_{k=0}^{n-1} H_k = \sum_{k=0}^{n-1} \omega \hbar N(k) \quad (29)$$

with the eigenvalue spectrum:

$$H |s_0, s_1, \dots, s_{n-1}\rangle = \omega \hbar \sum_{k=0}^{n-1} s_k |s_0, s_1, \dots, s_{n-1}\rangle \quad (30)$$

Having addressed the field theory, we now address the issue of the local (neuron-level) von Neumann entropy dynamics.

### 2.3 Entropy

Formally, in a QuANN, due to the networked nature of the quantum computation, the quantum dynamics at the local neuron level leads to entanglement between the neurons' quantum dynamics, which means that, locally, the neuron operates as an open quantum system. In general, with entanglement, we cannot describe the neuron in terms of a vector, but rather by a local density

operator, tracing out the rest of the network's degrees of freedom, which lead to the local (neuron-level) densities:

$$\rho_k(t) = Tr_k (|\psi(t)\rangle \langle\psi(t)|) \quad (31)$$

The quantum information dynamics of the network, at the local neuron level, can be addressed by calculating the von Neumann entropy with a binary basis, indeed considering the general formula:

$$S(\rho) = -Tr (\rho \log_2 \rho), \quad (32)$$

which is equal to 0 for a pure density, that is, a density given by a projector  $|\varphi\rangle \langle\varphi|$ , with  $|\varphi\rangle$  being a normalized vector, we can study the local neuron-level entropy dynamics employing similar recurrence analysis techniques as those introduced in the previous subsection, indeed, calculating the local von Neumann entropies for each neuron in binary basis we get the entropy sequences:

$$S_k(t) = S(\rho_k(t)) = -Tr (\rho_k(t) \log_2 \rho_k(t)) \quad (33)$$

that we can embed in  $\mathbb{R}^n$ ,  $(S_0(t), S_1(t), \dots, S_{n-1}(t))$ , and to which we can apply the recurrence analysis techniques in order to analyze the main dynamics for the local entropies.

When the input for the network is given by an initial pure density (a projector) the entropy for the full network is zero and remains zero under the evolution of the quantum neural map, since the map is unitary and therefore does not change the global entropy, the local neuron-level entropies, however, are not necessarily zero, due to the entanglement dynamics associated with quantum networked computation.

Since the neuron-level densities are usually not equal to a projector, there is usually some level of entropy fluctuations at the local neuron-level, indeed, the neuron-level networked dynamics tends to a far-from-equilibrium dynamics that does not stabilize in a fixed maximum entropy level, that is, while,



in certain iterations, the local neuron level's entropy can be led to close to the maximum entropy this is not always the case, and there can be entropy reductions to close to zero entropy, followed by entropy increases. In the case of class 4 dynamics, for instance, we can also get class 4 dynamics at the level of the entropy fluctuations themselves, with the entropy fluctuating in a fluctuation band that is not maximal.

Having introduced the main concepts and framework, we now address the example of the most elementary family of quantum recurrent neural networks (QRNNs) the QRNNs comprised of two neurons characterized by two-level neural firing activity (nonfiring and firing with a fixed energy level).

### 3 Complex Dynamics of a Quantum Recurrent Neural Network

#### 3.1 Structure of the Network

The most elementary QRNN is a network comprised of two neurons characterized by a two-level neural firing activity, which, following the previous section's formalism, is defined by:

$$G_{QRNN} = (\{n_0, n_1\}, \{(n_0, n_1), (n_1, n_0)\}, \mathbb{H}_2^{\otimes 2}, \Theta(\mathbb{H}_2^{\otimes 2})) \quad (34)$$

The neural firing pattern basis for this network is given by:

$$B_2^{\otimes 2} = \{|0, 0\rangle, |0, 1\rangle, |1, 0\rangle, |1, 1\rangle\} \quad (35)$$

The set of operators  $\Theta(H_{Net}) = \{U_0, U_1\}$  is, in turn, defined such that each operator is a conditional unitary operator that follows the neural connections, namely:

$$U_0 = U_{0,0} \otimes |0\rangle\langle 0| + U_{0,1} \otimes |1\rangle\langle 1| \quad (36)$$

$$U_1 = |0\rangle\langle 0| \otimes U_{1,0} + |1\rangle\langle 1| \otimes U_{1,1}, \quad (37)$$

where  $U_{r,s}$ , for  $r, s = 0, 1$ , are elements of the unitary group  $U(2)$ .

From the above equations, it follows that, under the connection  $(n_0, n_1)$ , the unitary gate  $U_{1,1}$  is applied at the second neuron when the first neuron is firing, while the unitary gate  $U_{1,0}$  is applied at the second neuron when the first neuron is nonfiring. In the reverse direction, a similar conditional computation is performed, so that when the second neuron is firing the computation at the first neuron is given by the operator  $U_{0,1}$  while, when the second neuron is nonfiring, the computation at the first neuron is given by the operator  $U_{0,0}$ .

Now, for a specific operator set  $\Theta(\mathbb{H}_{Net})$ , there are two possible activation orders for a unitary neural map  $U_1U_0$  or  $U_0U_1$ , the second alternative activates first the connection  $(n_0, n_1)$  and then the feedback (recurrent) connection  $(n_1, n_0)$ , the first alternative activates first the connection  $(n_1, n_0)$  and then the feedback (recurrent) connection  $(n_0, n_1)$ . In what follows, we will be working with the activation sequence  $U_0U_1$ .

The neural map that we will be analyzing has the following structure:

$$F = U_0U_1 \quad (38)$$

$$U_1 = |0\rangle\langle 0| \otimes I + |1\rangle\langle 1| \otimes U_r \quad (39)$$

$$U_0 = I \otimes |0\rangle\langle 0| + U_r \otimes |1\rangle\langle 1| \quad (40)$$

$$U_r = \cos\left(\frac{r\pi}{2}\right) (|0\rangle\langle 0| + |1\rangle\langle 1|) + \sin\left(\frac{r\pi}{2}\right) (-|0\rangle\langle 1| + |1\rangle\langle 0|) \quad (41)$$

In matrix representation, the two operators  $U_1$  and  $U_0$  are given by:

$$U_1 = \begin{pmatrix} 1 & 0 & 0 & 0 \\ 0 & 1 & 0 & 0 \\ 0 & 0 & \cos\left(\frac{r\pi}{2}\right) & -\sin\left(\frac{r\pi}{2}\right) \\ 0 & 0 & \sin\left(\frac{r\pi}{2}\right) & \cos\left(\frac{r\pi}{2}\right) \end{pmatrix} \quad (42)$$

$$U_0 = \begin{pmatrix} 1 & 0 & 0 & 0 \\ 0 & \cos\left(\frac{r\pi}{2}\right) & 0 & -\sin\left(\frac{r\pi}{2}\right) \\ 0 & 0 & 1 & 0 \\ 0 & \sin\left(\frac{r\pi}{2}\right) & 0 & \cos\left(\frac{r\pi}{2}\right) \end{pmatrix} \quad (43)$$

which leads to the following matrix structure of the neural map  $F$

$$F = \begin{pmatrix} 1 & 0 & 0 & 0 \\ 0 & \cos\left(\frac{r\pi}{2}\right) & -\sin^2\left(\frac{r\pi}{2}\right) & -\sin\left(\frac{r\pi}{2}\right)\cos\left(\frac{r\pi}{2}\right) \\ 0 & 0 & \cos\left(\frac{r\pi}{2}\right) & -\sin\left(\frac{r\pi}{2}\right) \\ 0 & \sin\left(\frac{r\pi}{2}\right) & \sin\left(\frac{r\pi}{2}\right)\cos\left(\frac{r\pi}{2}\right) & \cos^2\left(\frac{r\pi}{2}\right) \end{pmatrix} \quad (44)$$

Considering the Schrödinger picture iteration:

$$|\psi(t)\rangle = F |\psi(t-1)\rangle = U_0 U_1 |\psi(t-1)\rangle \quad (45)$$

and assuming the two expansions:

$$|\psi(t-1)\rangle = \sum_{s_0, s_1} \psi_{t-1}(s_0, s_1) |s_0, s_1\rangle \quad (46)$$

$$|\psi(t)\rangle = \sum_{s_0, s_1} \psi_t(s_0, s_1) |s_0, s_1\rangle \quad (47)$$

the amplitudes at  $t-1$  and at  $t$  are linked by:

$$\psi_t(0, 0) = \psi_{t-1}(0, 0) \quad (48)$$

$$\begin{aligned} \psi_t(0, 1) &= \cos\left(\frac{r\pi}{2}\right) \psi_{t-1}(0, 1) - \\ &- \sin^2\left(\frac{r\pi}{2}\right) \psi_{t-1}(1, 0) - \sin\left(\frac{r\pi}{2}\right) \cos\left(\frac{r\pi}{2}\right) \psi_{t-1}(1, 1) \end{aligned} \quad (49)$$

$$\psi_t(1, 0) = \cos\left(\frac{r\pi}{2}\right) \psi_{t-1}(1, 0) - \sin\left(\frac{r\pi}{2}\right) \psi_{t-1}(1, 1) \quad (50)$$

$$\begin{aligned} \psi_t(1, 1) &= \sin\left(\frac{r\pi}{2}\right) \psi_{t-1}(0, 1) + \\ &+ \cos\left(\frac{r\pi}{2}\right) \sin\left(\frac{r\pi}{2}\right) \psi_{t-1}(1, 0) + \cos^2\left(\frac{r\pi}{2}\right) \psi_{t-1}(1, 1) \end{aligned} \quad (51)$$

For  $r = 0$ ,  $\psi_t(s_0, s_1) = \psi_{t-1}(s_0, s_1)$ , so that we get a class 1 dynamics, that is, a fixed point, since  $|\psi(t)\rangle = |\psi(t-1)\rangle$ , so that the following holds:

$$|\psi(t)\rangle = |\psi(0)\rangle \quad (52)$$

for every normalized initial ket vector. With respect to the neural activity field, introduced in the previous section, we get the quantum averages:

$$\langle N(0) \rangle_t = |\psi_0(1, 0)|^2 + |\psi_0(1, 1)|^2 \quad (53)$$

$$\langle N(1) \rangle_t = |\psi_0(0, 1)|^2 + |\psi_0(1, 1)|^2 \quad (54)$$

which leads to a class 1 dynamics when the embedding in  $\mathbb{R}^2$  is performed, since the dynamical point for the mean field is a fixed point:

$$\langle N \rangle_t = (|\psi_0(1, 0)|^2 + |\psi_0(1, 1)|^2, |\psi_0(0, 1)|^2 + |\psi_0(1, 1)|^2) \quad (55)$$

On the other hand, when  $r = 1$ , the dynamics is class 2. The reason for this requires a closer look at the iteration steps, in this case from  $|\psi(t-1)\rangle$  to  $|\psi(t)\rangle$  we get the transition sequence:

$$\begin{aligned} |\psi(t)\rangle &= \psi_{t-1}(0, 0) |0, 0\rangle - \psi_{t-1}(1, 0) |0, 1\rangle - \\ &- \psi_{t-1}(1, 1) |1, 0\rangle + \psi_{t-1}(0, 1) |1, 1\rangle \end{aligned} \quad (56)$$

$$\begin{aligned}
|\psi(t+1)\rangle &= \psi_{t-1}(0,0)|0,0\rangle + \psi_{t-1}(1,1)|0,1\rangle - \\
&\quad - \psi_{t-1}(0,1)|1,0\rangle - \psi_{t-1}(1,0)|1,1\rangle
\end{aligned} \tag{57}$$

$$|\psi(t+2)\rangle = |\psi(t-1)\rangle \tag{58}$$

Therefore, we have a 3-cycle, that is, after three iterations, the ket vector returns to the configuration in which it was three iterations before, which leads to the embedded sequence:

$$\begin{aligned}
&\langle N \rangle_t = \\
&= (|\psi_{t-1}(1,1)|^2 + |\psi_{t-1}(0,1)|^2, |\psi_{t-1}(1,0)|^2 + |\psi_{t-1}(0,1)|^2)
\end{aligned} \tag{59}$$

$$\begin{aligned}
&\langle N \rangle_{t+1} = \\
&= (|\psi_{t-1}(0,1)|^2 + |\psi_{t-1}(1,0)|^2, |\psi_{t-1}(1,1)|^2 + |\psi_{t-1}(1,0)|^2)
\end{aligned} \tag{60}$$

$$\langle N \rangle_{t+2} = \langle N \rangle_{t-1} \tag{61}$$

While only class 1 and 2 dynamics are possible for these two parameters, more complex dynamics arise when  $0 < r < 1$ , for different initial conditions, as we now show.

### 3.2 Network Simulations

In figure 1, we show the simulated sequences for the mean neural activity field values at each neuron,  $\langle N(0) \rangle_t$  and  $\langle N(1) \rangle_t$ , when  $r = 0.0005$ , for  $|\psi(0)\rangle = |+\rangle \otimes |+\rangle$ , with  $|+\rangle = (|0\rangle + |1\rangle) / \sqrt{2}$ .

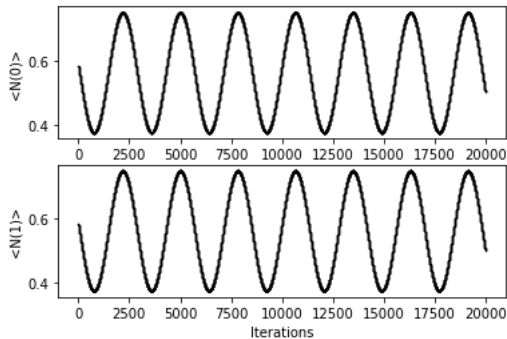


Figure 1: Simulation of the QRNN for  $r = 0.0005$ ,  $|\psi(0)\rangle = |+\rangle \otimes |+\rangle$ , with 20,000 iterations after 10,000 initial iterations being dropped for transients, the sample correlation between the two neurons' values for the mean neural activity field is 0.99999977.

In this case, we get an emergent pattern which follows a sinusoidal curve for both neurons, with a high level of synchronization in the sinusoidal pattern between the two neurons.

It is important to stress that the plot in figure 1 is actually a scatterplot, the appearance of a continuous periodic curve is due to the close proximity of the dots, which means that the sinusoidal pattern holds as an emergent pattern that appears in the dots' sequence for each iteration.

The sequence of dots is actually quasiperiodic, since for a recurrence radius of 0 we get a recurrence probability equal to 0, however, the quasiperiodicity is following an emergent continuous periodic curve, that is, we get an emergent brainwave-like pattern that determines the dynamics at the level of the mean field at each neuron which, while being quasiperiodic, follows, in fact, an emergent continuous periodic shape. Since the two emergent periodic curves are synchronized, we get a pattern that is like an emergent synchronized neural wave driving the network's dynamics.

While  $r = 0$  leads to a fixed point dynamics, increasing the parameter to  $r > 0$ , for low values of this parameter we get an emergent "brainwave" for different initial conditions.

In figure 2, we show the corresponding sequences of mean neural activity field values at each neuron for the initial conditions  $|\psi(0)\rangle = |0, 1\rangle$ ,  $|\psi(0)\rangle = |1, 0\rangle$  and  $|\psi(0)\rangle = |1, 1\rangle$ , and  $r = 0.0005$ , in all three cases we get an emergent pattern that is like a continuous wave, with a high correlation between the mean field dynamics, however, for the first two cases, the sample correlation is negative, which corresponds to a neural inhibitory dynamics, while for the last case it is positive, corresponding to a neural reinforcing dynamics. In the inhibitory cases this leads to an emergent negatively correlated excitation-relaxation cycle between the two neurons with a plateau in the excited phase and a smooth but faster relaxation phase.

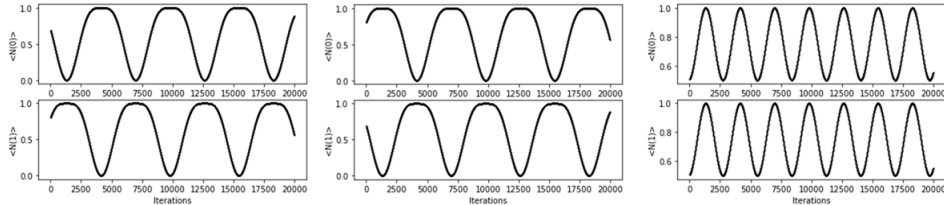


Figure 2: Simulations of the QRNN for  $r = 0.0005$ , with 20,000 iterations after 10,000 initial iterations being dropped for transients, and with initial conditions given by  $|\psi(0)\rangle = |0, 1\rangle$  (left),  $|\psi(0)\rangle = |1, 0\rangle$  (middle) and  $|\psi(0)\rangle = |1, 1\rangle$  (right), in the first case, the sample correlation is  $-0.87907088$ , in the second  $-0.87906459$  and in the third  $0.99999955$

The dynamics, shown in figures 1 and 2 are also characterized by emergent continuous periodic dynamics driving the neurons' entanglement dynamics with a signature at the von Neumann entropy levels, which is different from Everett's quantum automaton dynamics where the entanglement leads to a fixed branching entanglement pattern (Everett, 1957, 1973), the difference is that Everett's quantum automata theory is linked to a formalization of a laboratory-based theory of quantum measurement, and the measurement is a feedforward single interaction between the observer and the observed system plus apparatus, in this sense at the level of the observer's description there is an entanglement-related local decoherence (Tegmark, 2000; Joos *et*

*al.*, 2003).

In QuANNs there is, however, no fixed/stable decoherence identifiable as a von Neumann entropy rise to a fixed local maximally mixed density, instead, due to the networked interaction, the entropy fluctuates, so we do not have the same type of framework as is assumed in Everett (1957, 1973) regarding quantum cognition, which, as stated, is an expansion from a laboratory-based framework focused on a specific type of interaction which is a quantum measurement, instead, for QuANNs, we need to consider the issue of complex entropy dynamics associated with interacting quantum systems in order to address quantum networked processing at the local neuron level, where each neuron's computational dynamics operates far-from-equilibrium.

In order to better understand this point, let us consider the local neuron description. In the case of the above network, the local neuron-level entropy, like the mean neural activity field, is also driven by an emergent periodic continuous dynamics and exhibits a complex dynamical relation with respect to the mean field values as we show in figure 3, for  $|\psi(0)\rangle = |+\rangle \otimes |+\rangle$ . In this case, the initial entropy for each neuron was zero, since the input vector for the network was separated into a tensor product of two ket vectors. As the iterations proceed, we find that even though the entropy sequence is discrete, like the mean neural activity field values, it follows a continuous smooth curve which is periodic in pattern, the entropy fluctuations range from near zero entropy which corresponds to a pure density, to near 1, which corresponds to a maximum entropy level associated with a depolarized mixed density, the mean entropy being around 0.63 bits, as shown in table 1.



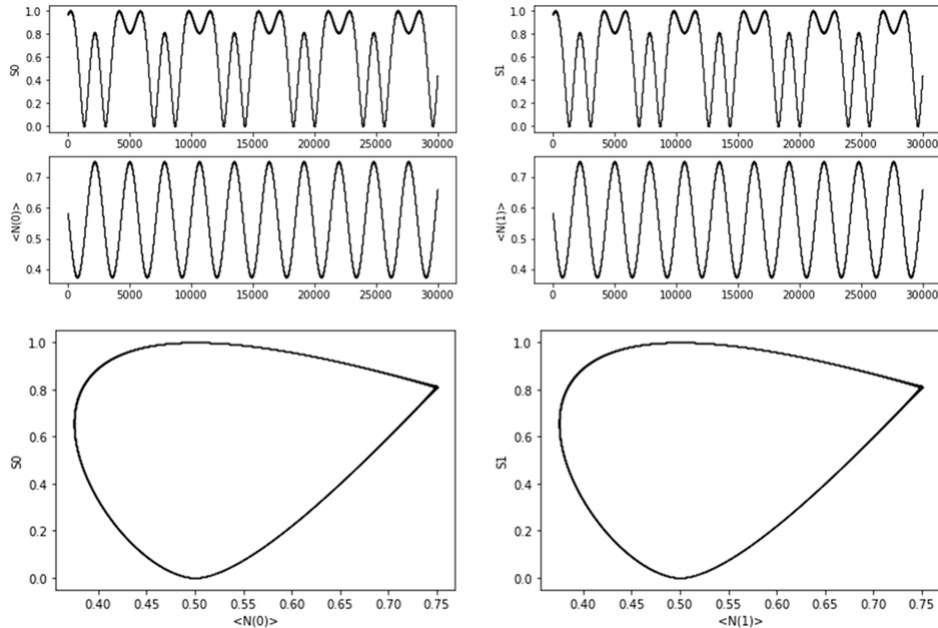


Figure 3: Simulations of the QRNN for  $r = 0.0005$ , with comparison between the mean neural activity field dynamics and the corresponding von Neumann entropy values at neuron  $n_0$  (left) and neuron  $n_1$  (right), with 30,000 iterations after 10,000 initial iterations being dropped for transients, and with initial condition given by  $|\psi(0)\rangle = |+\rangle \otimes |+\rangle$ .

	$n_0$	$n_1$
Minimum Entropy	8.0281238e-09	8.0278112e-09
Maximum Entropy	0.9999998	0.9999998
Mean Entropy	0.6347909	0.6347909

Table 1: Main entropy statistics for figure 3's simulation

There is also a relation between the mean neural activity field at each neuron and the respective entropy, in this case, we get an eye-like structure, such that when the mean field value at the neuron is near 0.5, the entropy is either near 0 or near 1. For higher values of the mean neural activity field, the dispersion in entropy fluctuations diminish converging on a high

but non-maximal entropy value for the maximum mean neural activity field value, which also corresponds to maximum mean energy at the neuron level.

Throughout the network’s iterations each neuron is operating as an open quantum computing system with fluctuations in entropy that can range from a value close to zero to a value close to the maximum entropy level, which illustrates the point that we do not get the basic fixed decoherence pattern that is addressed in the context of quantum measurement theory (Everett, 1957, 1973; Tegmark, 2000; Joos *et al.*, 2003). This is also the case for the entropy dynamics associated with the initial conditions of figure 2.

Emergent smooth periodic curves driving the mean neural activity field and entropy values are not the only patterns that are present in this network’s dynamics. When the network is initialized for  $|\psi(0)\rangle = |+\rangle \otimes |+\rangle$ , as  $r$  is increased, in the region of periodic emergent brainwave-like patterns, the wavelength of the resulting neural waves decreases, so that for  $r$  very near 0, the wavelength is longer, but, as  $r$  is increased, the wavelength decreases, as well as the sample correlation. As shown in Gonçalves (2020), these correlations eventually transition from from positive to negative values, with two main shapes characterizing the dynamics of the mean neural activity field at neuron  $n_0$  versus at neuron  $n_1$ , one with a triketa-like shape<sup>1</sup> and the other with the shape of a trifolium, with the transition from the triketa to the trifolium being progressive as  $r$  is increased, exhibiting complex quasiperiodic dynamics. Two examples of these attractors are shown in figure 4.

---

<sup>1</sup>It can be obtained from intersections of three ellipsoids.

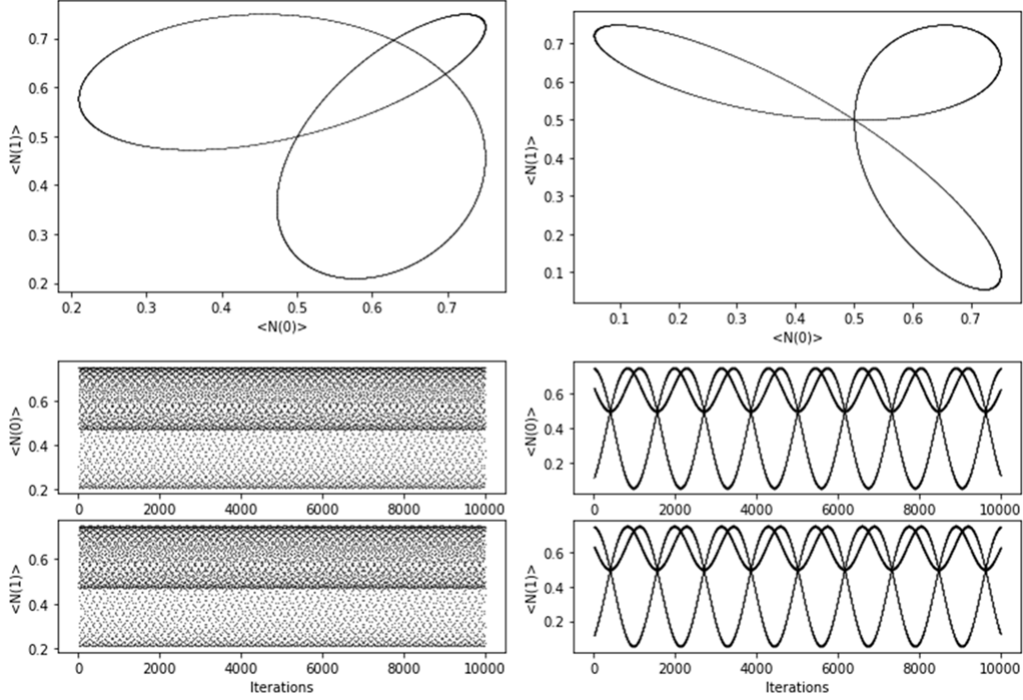


Figure 4: Attractor plots, showing the mean neural activity field at neuron  $n_0$  versus at neuron  $n_1$ , for  $r = 0.550129597$  (left) and  $r = 0.999$  (right), with 10,000 iterations after 10,000 initial iterations being dropped for transients and initial condition given, in both cases, by  $|\psi(0)\rangle = |+\rangle \otimes |+\rangle$ , also shown are the respective iterations graphs with the time series sequences for the mean neural activity field values.

The attractor on the left corresponds to a value of  $r$  where the two neurons show a close to zero correlation<sup>2</sup>, while, for the attractor on the right, the correlation is negative<sup>3</sup>. While positive correlation indicates a dominance of an excitatory dynamics between the two neurons, and a negative correlation indicates the presence of an inhibitory relation, in the close to zero and negative correlation region, unlike the positive correlation region, the dynamics is characterized by complex quasiperiodic structures, mainly the

<sup>2</sup>In this case, the sample correlation for figure 4's simulation is  $1.85638176e-05$ .

<sup>3</sup>In this case, the sample correlation for figure 4's simulation is  $-0.49961075$ .

triketa which is the dominant geometrical structure, with the trifolium only emerging for  $r$  greater than 0.99. It is important to stress that even though we get the same triketa shape, different values of the parameter  $r$  lead to different complex quasiperiodic patterns with different recurrence structures as systematized in Gonçalves (2020).

The nonlinear relation between the sequences of mean field values at each neuron emerges as  $r$  increases, and the triketa becomes the dominant emergent dynamical geometry both for near zero correlation and negative correlation. In this sense, the linear correlation measure becomes misleading as measure of the relation between the mean neural activity field at each neuron.

This point becomes particularly relevant when considering the near zero correlation case, since, while there is no dominant excitatory or inhibitory dynamics, there is still a nonlinear relation between the neurons which is characterized by a dynamics that exhibits, in the recurrence structure, both signatures of dynamics with multiple periodicities characterized by long resilient diagonals with 100% recurrence as well as broken diagonals and isolated dots that ususally appear in stochastic or chaotic systems.

The dynamics is actually not chaotic nor periodic, instead, it is closer, in regards to the recurrence structure, to the *edge of chaos*, such types of dynamics have been identified in other QuANN models including recurrent networks interacting with an environment (Gonçalves, 2017), as reviewed in the introduction. The recurrence plots for the near zero correlation case are shown in figure 5, illustrating this point.

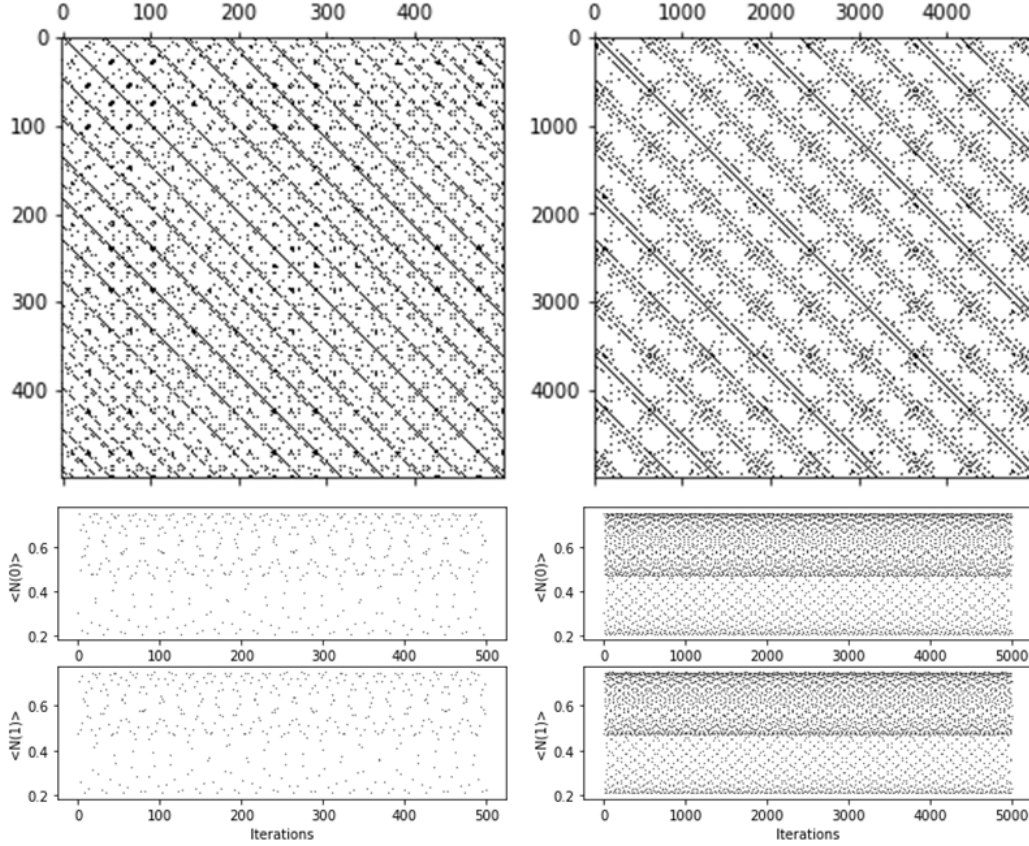


Figure 5: Sequence of mean field values at each neuron and recurrence plots obtained for the ordered pairs  $(\langle N(0) \rangle_t, \langle N(1) \rangle_t)$ ,  $r = 0.550129597$ , 500 iterations (left) and 5,000 iterations (right), after 10,000 initial iterations being dropped for transients, the radius used for the recurrence plot was 0.1, the distance used was the Euclidean distance, with recurrence points plotted in black and initial condition given, in both cases, by  $|\psi(0)\rangle = |+\rangle \otimes |+\rangle$ .

As can be seen in figure 5, we no longer have the sequence of mean field values following an emergent continuous periodic pattern, instead, we get a dispersion in the form of a cloud of points, with the complex pattern only being visible for higher number of iterations. The *edge of chaos* recurrence signatures show up upon an analysis of the recurrence quantification measures.

In table 2, we show the results from a recurrence analysis on the ordered pairs  $(\langle N(0) \rangle_t, \langle N(1) \rangle_t)$ , for 20,000 iterations after 10,000 initial iterations being dropped for transients, with  $r = 0.550129597$ .

Radius	Recurrence Probability	Mean Recurrence Strength	P[100% Rec Rec]
0	0	-	-
0.001	0.006750	0.116914	0.081481
0.01	0.069303	0.126819	0.086580
0.02	0.140057	0.129167	0.085684
0.03	0.211161	0.132081	0.085721
0.04	0.284464	0.134353	0.084725
0.05	0.360418	0.136247	0.083657
0.06	0.439772	0.137854	0.082661
0.07	0.525426	0.138656	0.080415
0.08	0.621031	0.138282	0.077939
0.09	0.737737	0.135577	0.073946
0.1	0.941097	0.123607	0.064502

Table 2: Recurrence plot statistics for the ordered pairs  $(\langle N(0) \rangle_t, \langle N(1) \rangle_t)$ , obtained from 20,000 iterations simulations after 10,000 initial iterations being dropped for transients, with  $r = 0.550129597$ , initial condition  $|\psi(0)\rangle = |+\rangle \otimes |+\rangle$ , the statistics were calculated for increasing radius using a Euclidean metric.

The table shows how the recurrence statistics change with the increasing radius, for radius 0, the recurrence probability is zero since there are no diagonals, below the main diagonal, with recurrence, which is indicative of an nonperiodic dynamics, the recurrence probability and the mean recurrence strengths rise with the radius reaching a 94.1097% recurrence probability for the radius 0.1, the probability of finding a diagonal line with 100% recurrence conditional on the diagonal having recurrence points, however, rises initially with the radius but then starts dropping, this indicates that the new recurrence points that appear with the rise in radius are predominantly isolated and clustered dots more characteristic of a noisy recurrence structure, in this case, there is a resilient quasiperiodic skeleton of lines with 100% recurrence,

but the remaining recurrence points do not tend to produce a 100% recurrence, which leads to a mix of an emergent stochastic-like recurrence pattern intermixed with a few long diagonals, characterizing a complex quasiperiodic dynamics, this is characteristic of *edge of chaos* signatures.

To evaluate the periodicities involved, we can calculate the distances between the 100% recurrence lines, these distances provide for an evaluation of the quasiperiodic skeleton, in this case, for a radius of 0.1, we find the present of three cycles, a 5 iterations cycle, a 21 iterations cycle and a 26 iterations cycle, the fact that there are different cycles present is characteristic of quasiperiodic dynamics, in this case, there are two dominant cycles, for a radius of 0.1, the first is the 21 iterations cycle, which occurs 836 times, followed by the 5 iterations cycle which occurs 352 times, by contrast, the 26 iterations cycle only appears 25 times, as shown in table 3.

Distances	Frequencies	%
5	352	29.019%
21	836	68.920%
26	25	2.061%

Table 3: Distances between 100% recurrence lines' statistics for the ordered pairs  $(\langle N(0) \rangle_t, \langle N(1) \rangle_t)$ , obtained from 20,000 iterations simulations after 10,000 initial iterations were dropped for transients, with  $r = 0.550129597$ , initial condition  $|\psi(0)\rangle = |+\rangle \otimes |+\rangle$ , the statistics were calculated for a radius of 0.1 using a Euclidean metric.

Now, if we consider the von Neumann entropy dynamics, for  $r = 0.550129597$ , we need to consider the sequences of entropy values associated with neurons  $n_0$  and  $n_1$ , respectively,  $S_0(t)$  and  $S_1(t)$ , calculated from the respective neuron-level reduced densities, as shown in figure 6 we also get a nonperiodic dynamics, with multiple diagonals but also a high number of interrupted diagonals and isolated clusters, the power spectrum has multiple spikes at the high frequency level for both neurons entropy sequences.

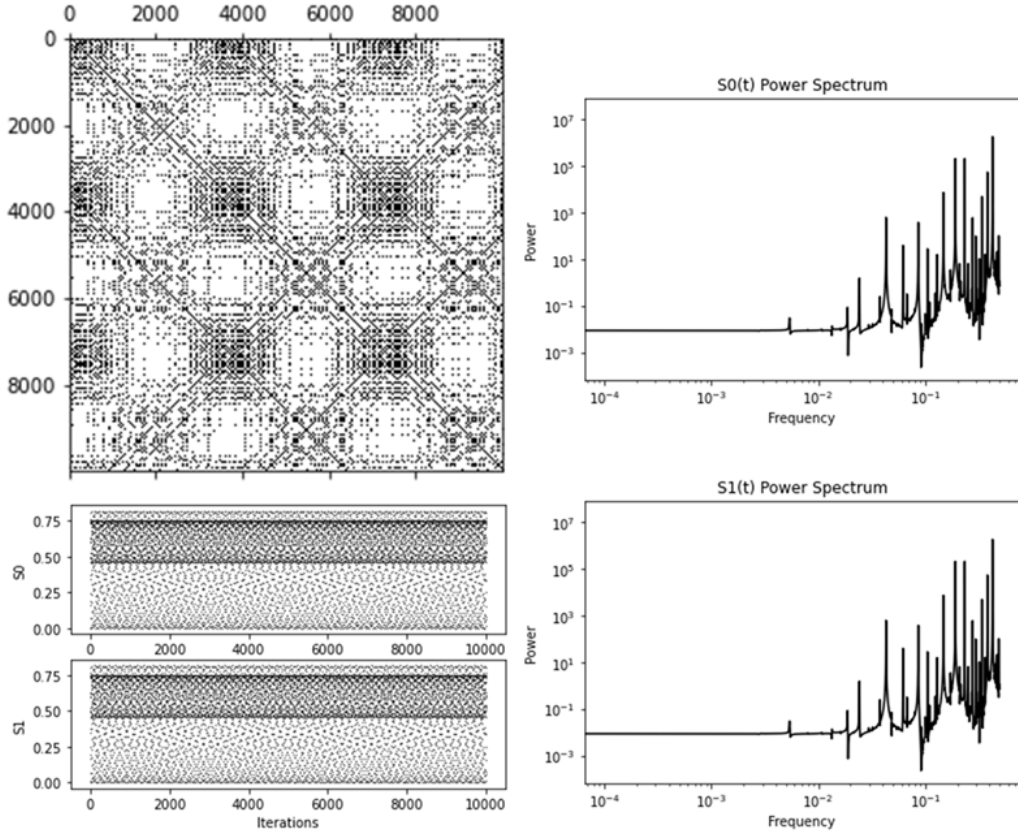


Figure 6: Sequences of entropy values  $S_0(t)$  and  $S_1(t)$  associated, respectively, with neuron  $n_0$  and  $n_1$ , with  $r = 0.550129597$ , recurrence plot obtained for the ordered pairs  $(S_0(t), S_1(t))$  and power spectrum associated with each entropy sequence, 10,000 iterations were plotted, after 10,000 initial iterations being dropped for transients, the radius used for the recurrence plot was 0.1, the distance used was the Euclidean distance, with recurrence points plotted in black, and initial condition given by  $|\psi(0)\rangle = |+\rangle \otimes |+\rangle$ .

There is, in this case, a predominant cycle which corresponds to a 47 iterations cycle that occurs 248 times with respect to the 100% recurrence lines at a radius of 0.1, the second cycle, in importance, is a 68 iterations cycle, that occurs 88 times and a 115 iterations cycle, that occurs 20 times, as shown in table 4.



Distances	Frequencies	%
47	248	69.663%
68	88	24.719%
115	20	5.618%

Table 4: Distances between 100% recurrence lines' statistics for the ordered pairs  $(S_0(t), S_1(t))$ , obtained from 20,000 iterations simulations after 10,000 initial iterations being dropped for transients, with  $r = 0.550129597$ , initial condition  $|\psi(0)\rangle = |+\rangle \otimes |+\rangle$ , the statistics were calculated for a radius of 0.1 using a Euclidean metric.

Given the above results, we do not have, again, the stabilization in a fixed entropy regime, the entropy fluctuations exhibit a complex dynamics, associated with changes in entanglement levels and quantum amplitudes.

As shown in table 5, the lowest entropy value is close to zero, while the highest entropy value is around 0.819 bits, no neuron is ever led to the maximum entropy level associated with a depolarized mixed density, and the mean entropy is around 0.498, so each neuron is operating as a far-from-equilibrium open quantum system.

	$n_0$	$n_1$
Minimum Entropy	2.2997412e-08	2.2997181e-08
Maximum Entropy	0.8191482	0.8191481
Mean Entropy	0.4976293	0.4976293

Table 5: Main entropy statistics for figure 6's simulation.

For  $r = 0.999$ , the entropy also has a complex pattern, as shown in figure 7.

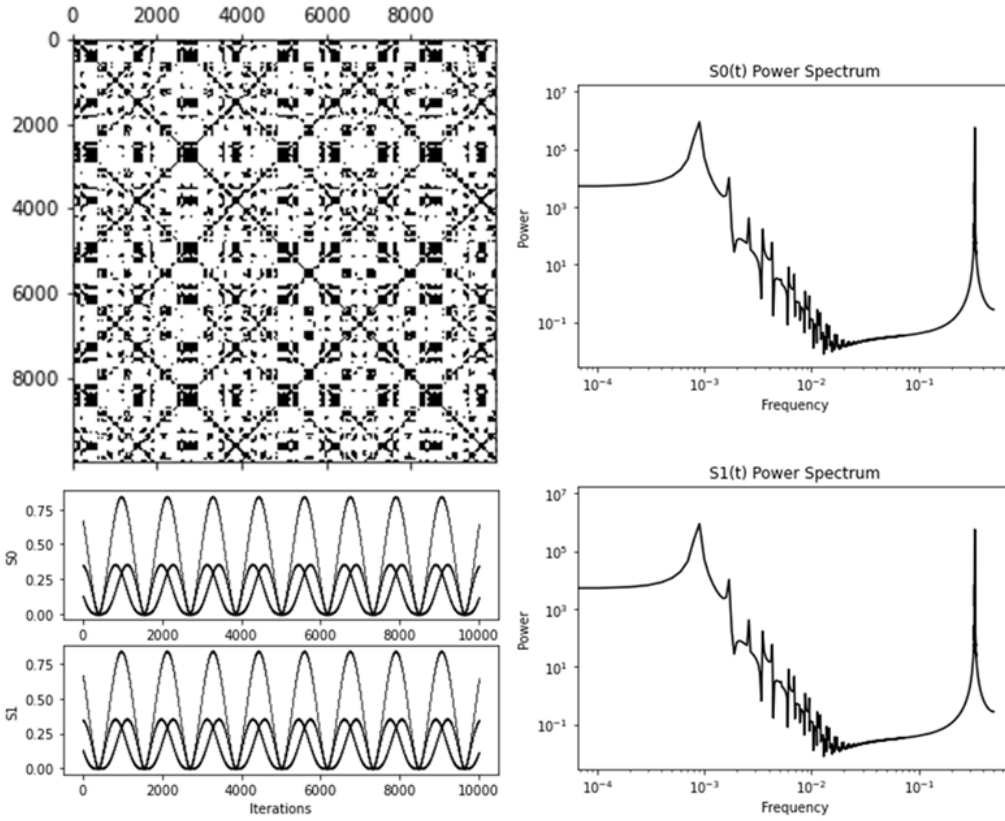


Figure 7: Sequences of entropy values  $S_0(t)$  and  $S_1(t)$  associated, respectively, with neuron  $n_0$  and  $n_1$ , with  $r = 0.999$ , recurrence plot obtained for the ordered pairs  $(S_0(t), S_1(t))$  and power spectrum associated with each entropy sequence, 10,000 iterations were plotted, after 10,000 initial iterations being dropped for transients, the radius used for the recurrence plot was 0.1, the distance used was the Euclidean distance, with recurrence points plotted in black.

While, in figure 7, the entropy series values follow an emergent smooth complex periodic curve, the process is very nontrivial, indeed, working with the power spectrum, we find the presence of a power law decay in the spectrum obtained for the von Neumann entropy sequences  $S_0(t)$  and  $S_1(t)$  with an additional rise for a significant peak at the high frequency scale, indicating the presence of a strong periodicity at that higher frequency. The recurrence

plot shows elements of a periodic skeleton but also local neighborhood fluctuations in the sequence.

	$n_0$	$n_1$
Minimum Entropy	9.5207835e-09	9.5208386e-09
Maximum Entropy	0.8427277	0.8427277
Mean Entropy	0.2608883	0.2608883

Table 6: Main entropy statistics for figure 7’s simulation

As shown in table 6, the interval of values for the entropy fluctuations is similar to the previous one, the lowest entropy value is close to zero, the highest entropy value is around 0.843 bits, the mean entropy is, however, lower than in the previous case, around 0.261 bits, again, no neuron is ever led to the maximum entropy level and each neuron is computing far from the maximum entropy level.

## 4 Discussion

In the present work we introduced a formalism for studying QuANNs as complex quantum dynamical systems, demanding the introduction of a quantum field theory on a quantum computing network and an expansion of the concept of unitary map, worked within quantum chaos theory, to the quantum computer science context of QuANNs and expanded further to the quantum computing field theory.

The simulation of QuANNs as dynamical systems shows a diversity of complex dynamics, even in small networks. For the most basic QRNN, a network comprised of just two neurons, we obtained a diversity of complex regimes in the quantum computational field dynamics that matches the dynamical classes identified in classical networked computational models studied within classical complexity sciences, and leads to each neuron operating as a far-from-equilibrium open quantum system.

In the current work, we showed that dynamical classes, researched upon in the classical complexity sciences in regards to networked evolutionary computing systems' dynamics, characterize not only the quantum mean neural activity field dynamics but also the local entropy sequences, which differentiates between QuANNs operating as quantum computing networked dynamical systems from another class of quantum automata worked by Everett (1957; 1973) to address a type of measurement-like interaction where the entropy for the local system rises to a fixed level marked by a local diagonalization of the local density, which has characterized the decoherence by interaction with the environment literature (Tegmark, 2000; Joos *et al.*, 2003). When linked in network, each neuron operates as an open quantum computing system, exhibiting entropy fluctuations that can get close to zero and, in the case of the studied class 4 emergent quantum neural computing field dynamics, never achieve a maximum entropy value.

Further research is needed into QuANNs as dynamical systems, both in regards to the formalism of quantum computing field theory and in regards to the simulation of these networks, especially with the addition of more neurons and connections. From a computer science standpoint, such a research may provide new results into low decoherence far-from-equilibrium complex networked quantum computing systems with possible applications in nanotechnology, quantum biology research, quantum computing, quantum internet and A.I. research. Also, the far-from-equilibrium class 4 dynamics leads to the emergence of a form of resilient dynamical memory encoded in the sequence of quantum averages, as resilient recurrences, which may open up a research route into quantum dynamical memory storage.

Another implication of the results obtained from the simulations is the need for a dialogue with neuroscience, considering especially the fact of the emergence of brainwave-like patterns with different wavelengths and the possibility of including network adaptive response to signals leading to different wavelength responses at the quantum neural activity level.

## References

- Acharya** UR, Sree SV, Chattopadhyay S, Yu W, Ang PC. Application of recurrence quantification analysis for the automated identification of epileptic EEG signals. *Int. J. Neural Syst.*, 2011, 21(3): 199-211.
- Aladag** CH, Egrioglu E, Kadilar C. Modeling Brain Wave Data by Using Artificial Neural Networks. *Hacettepe Jour. of Math. and Stat.*, 2010, 39(1): 81-88.
- Beer** K, Bondarenko D, Farrelly T, Osborne TJ, Salzmann R, Scheiermann D, Wolf R. Training deep quantum neural networks. *Nature Communications*, 2020; 11: 808.
- Braun**, D. *Dissipative Quantum Chaos and Decoherence*. Springer, Berlin, 2001.
- Cramer** JG. *The Quantum Handshake: Entanglement, Nonlocality and Transactions*. Springer, Switzerland, 2016.
- Dupuy** J-P. *The Mechanization of the Mind*, Translation by MB DeBevoise, Princeton University Press, Princeton, 2000.
- Eckmann**, J-P; Kamphorst, SO; Ruelle, D. Recurrence Plots of Dynamical Systems. *Europhys. Lett.*, 1987, 4(9): 973-977.
- Everett** H. 'Relative state' formulation of quantum mechanics. *Rev. of Mod. Physics*, 1957; 29(3): 454-462.
- Everett** H. *The Theory of the Universal Wavefunction*, PhD Manuscript, In: DeWitt R and Graham N (eds.), *The Many-Worlds Interpretation of Quantum Mechanics*. Princeton Series in Physics, Princeton University Press, Princeton, 1973, 3-140.

- Gao** J and Cai H. On the Structures and Quantification of Recurrence Plots. *Phys. Lett.*, 2000, A270: 75-87.
- Gonçalves** CP. Quantum Cybernetics and Complex Quantum Systems Science - A Quantum Connectionist Exploration. *NeuroQuantology* 2015a; 13(1): 35-48.
- Gonçalves** CP. Financial Market Modeling with Quantum Neural Networks. *Review of Business and Economics Studies* 2015b; 3(4):44-63.
- Gonçalves** CP. Quantum Neural Machine Learning: Backpropagation and Dynamics. *NeuroQuantology*, 2017; 15(1): 22-41.
- Gonçalves** CP. Quantum Robotics, Neural Networks and The Quantum Force Interpretation. *NeuroQuantology*, 2019a; 17(2): 33-55.
- Gonçalves** CP. Quantum Neural Machine Learning - Theory and Experiments. Aceves-Fernandez, M.A. (Ed.). *Machine Learning in Medicine and Biology*. IntechOpen, London, 2019b: 95-118.
- Gonçalves** CP. Quantum Stochastic Neural Maps and Quantum Neural Networks. *Neurobiology eJournal* 4(3), *Computational Biology eJournal* 4(4) and *Information Systems eJournal* 3(9) (SSRN), 2020; doi: 10.2139/ssrn.3502121. Accessed date: February 2, 2022.
- Gorodkin** J, Sørensen A, Winther O. Neural Networks and Cellular Automata Complexity. *Complex Systems*, 1993; 7:1-23.
- Houssein** EH, Abohashima Z, Elhoseny M, Mohamed WM. Machine learning in the quantum realm: The state-of-the-art, challenges, and future vision. *Expert Systems with Applications* 2022; 194: 116512.
- Ivancevic** VG, Reid DJ, Pilling MJ. *Mathematics of Autonomy: Mathematical Methods for Cyber-Physical-Cognitive Systems*. World Scientific, World Scientific, Singapore, 2018.

- Joos** E, Zeh HD, Kiefer C, Giulini D, Kupsch J, Stamatescu I-O (Eds.). Decoherence and the Appearance of a Classical World in Quantum Theory. Springer, Germany, 2003.
- Kauffman** SA and Johnsen S. Coevolution to the Edge of Chaos: Coupled Fitness Landscapes, Poised States, and Coevolutionary Avalanches. *J Theor Biol* 1991; 149:467- 505.
- Kauffman** SA. The Origins of Order: Self-Organization and Selection in Evolution. Oxford University Press, New York, 1993.
- Kwak** Y, Yun WJ, Jung S, Kim J. Quantum Neural Networks: Concepts, Applications, and Challenges. IEEE, *Twelfth International Conference on Ubiquitous and Future Networks (ICUFN)*, 2021:413-416.
- Langton** C. Computation at the Edge of Chaos: Phase Transitions and Emergent Computation. *Physica D* 1990; 42:12-37.
- Lopes** MA, Zhang J, Krzemiński D, Hamandi K, Chen Q, Livi L, Masuda N. Recurrence quantification analysis of dynamic brain networks. *Eur J Neurosci.* 2021, 53: 1040–1059.
- Novikov** DA. Cybernetics: From Past to Future. Springer, Switzerland, 2016.
- Packard**, NH. Adaptation toward the edge of chaos. University of Illinois at Urbana-Champaign, Center for Complex Systems Research, 1988.
- Parisi** L, Neagu D, Ma R, Campean IF. Quantum ReLU activation for Convolutional Neural Networks to improve diagnosis of Parkinson’s disease and COVID-19. *Expert Systems with Applications*, 2022; 187: 115892.
- Stöckmann** H-J. Quantum Chaos - an introduction. Cambridge University Press, UK, 2000.

**Tegmark** M. Importance of quantum decoherence in brain processes. Phys Rev E, 2000; 61(4):4194-4206.

**Thomasson** N, Webber CL Jr, Zbilut JP. Application of recurrence quantification analysis to EEG signals. Int. J. Comp. Appl., 2002, 9: 1-6.

**Wolfram** S. A New Kind of Science. Wolfram Media, USA, 2002.